frontiers in Energy Research

ORIGINAL RESEARCH
published: 28 April 2020
doi: 10.3389/fenrg.2020.00052

High-Temperature Treatment to Improve the Capacity of LiBC Anode Material in Li-ion Battery

Qianwen Yang, Langlang Chen, Xiang Feng, De Li and Yong Chen**

State Key Laboratory on Marine Resource Utilization in South China Sea, Hainan Provincial Key Laboratory of Research on Utilization of Si-Zr-Ti Resources, School of Materials Science and Engineering, Hainan University, Haikou, China

Being a graphite-like material, LiBC can deliver a high capacity as an anode material in Li-ion batteries, which are strongly dependent on carbon precursors. Developing a method to improve the capacity would be significant to the study and utilization of LiBC anode material. Here we treated a pristine LiBC material with a high temperature to obtain four modified LiBC samples. A reversible capacity of 353 mAh/g was delivered by a modified LiBC sample treated at 600°C for 10 h in a powder form wrapped with an Al foil, which was only 218 mAh/g for the pristine LiBC in Li-ion batteries. According to the XRD result, the layer structure of LiBC was maintained after the high-temperature treatment, while the lattice parameters were changed slightly, especially for the interlayer distance. The modified LiBC samples showed a similar Raman spectra to the pristine LiBC except for the peak intensity, which indicates lithium evaporation during high-temperature treatment. Thereby, the high-temperature treatment can improve the capacity of LiBC through reducing the lithium content and modifying the crystal structure, and this method would make the LiBC material become a more promising anode material in Li-ion batteries.

Keywords: Li-ion battery, LiBC, graphite, high-temperature treatment, capacity, anode material

OPEN ACCESS

Edited by:
Wei-Ren Liu,
Chung Yuan Christian University, Taiwan

Reviewed by:
Liqiang Mai,
Wuhan University of Technology, China
Zhumabay Bakenov,
Nazarbayev University, Kazakhstan
Xifei Li,
Xi'an University of Technology, China

****Correspondence:***
De Li
lidenju@sina.com
Yong Chen
ychen2002@163.com

Specialty section:
This article was submitted to Electrochemical Energy Conversion and Storage, a section of the journal Frontiers in Energy Research

Received: *13 January 2020*
Accepted: *16 March 2020*
Published: *28 April 2020*

Citation:
Yang Q, Chen L, Feng X, Li D and Chen Y (2020) High-Temperature Treatment to Improve the Capacity of LiBC Anode Material in Li-ion Battery. Front. Energy Res. 8:52. doi: 10.3389/fenrg.2020.00052

INTRODUCTION

In order to protect the environment, a lot of effort has been put into the development of renewable energy, even as it is a big challenge to produce a compatible energy storage system. The rechargeable Li-ion battery is a promising choice for the storage of renewable energy in smart power grids, and it has been widely used in portable electronic devices and electric vehicles (Ohzuku et al., 1993; Armand and Tarascon, 2008; Van Noorden, 2014). A large number of new materials have been developed for electrode materials or for improving the performance of batteries (Shan et al., 2016; Xiong et al., 2018). Up to now, graphite with a theoretical capacity of 372 mAh/g is the predominant anode material in commercial Li-ion batteries, although many other anode materials with high capacities have attracted a lot of interest. Lithium ions can reversibly intercalate into the layered graphite, of which the carbon atoms are hexagonally bonded through the sp^2 hybridization (Chevallier et al., 2013). Considering their stable structure and light weight, it is still a very promising prospect to develop from graphite-like materials a next-generation anode material which would combine the superiority of graphite and a higher capacity.

In carbon boron substitution, the capacity of graphite can be evidently improved due to the contribution of doped boron (Way, 2010). Hexagonal BC_3 was theoretically predicted to have

a high-capacity for Li, Na, and K Ion batteries (Kuzubov et al., 2012; Van Noorden, 2014; Joshi et al., 2015; Belasfar et al., 2020). A low-crystalized BC_3 material was experimentally synthesized and electrochemically measured, which delivered a good Li-storage capacity (King et al., 2013, 2015). When the boron content was further increased to the same as that of carbon, the graphite evolved into a new material as LiBC, which has a similar structure to MgB_2 (An and Pickett, 2001). In a typical LiBC structure, the BC layers are formed by the B–C bonding in an sp^2 configuration, which are stacked with antiparallel B–C bonds, and Li ions are sited in-between BC layers (Woerle et al., 1995; Bharathi et al., 2002; Fogg et al., 2003, 2006, 2008; Souptel et al., 2003; Zhao et al., 2003; Renker et al., 2004; Krumeich et al., 2014). The domain structure and stacking faults may exist in lithium-deficient LiBC (Kalkan and Ozdas, 2019). Through computational simulations within density functional theory, Xu et al. predicted a reversible electrochemical reaction of $LiBC \rightleftharpoons Li_{0.5}BC + 0.5Li$ in the LiBC as a cathode material (Xu et al., 2011), while Langer et al. experimentally proved the poor electrochemical performance of LiBC as an electrode material (Langer et al., 2012).

In our previous work (Jia et al., 2018; Li et al., 2018), we synthesized the LiBC material with a carbon precursor of acetylene black, which delivered a high reversible capacity of 500 mAh/g in Li-ion batteries. The specific capacity of LiBC was very dependent on the carbon precursor, which is only about 200 mAh/g for a carbon precursor of graphite. In this work, we treated a pristine LiBC material with a high temperature to make its reversible capacity increase from 218 to 353 mAh/g. According to the XRD and Raman results, some lithium was evaporated from the LiBC material and the interlayer distance was increased slightly during the high-temperature treatment, which might give rise to the higher capacity of modified LiBC samples.

EXPERIMENTAL SECTION

Materials Synthesis

Pristine LiBC material (Sample I) was synthesized from the raw materials as LiH (≥97.0%, Shanghai Macklin Biochemical Co., Ltd), amorphous B (≥95.0%, Sigma-Aldrich Co. LLC), and graphite (750 mesh, 99.99%, Shanghai Aladdin Biochemical Technology Co., Ltd) with a mole ratio of LiH: B : C = 1: 1: 1. In an Ar atmosphere, the raw materials were thoroughly ground in an agate mortar, pressed into a pellet, sandwiched by two Ta discs, and loaded within a stainless steel vessel, as shown in the top of **Figure 1**. In a quartz tube furnace with an Ar atmosphere, the vessel was calcined at 800°C for 10 h to produce the LiBC sample. The LiBC sample was taken out from the vessel and stored inside a glove box with Ar gas (H_2O, O_2 < 1 ppm). As shown in the bottom of **Figure 1**, the pristine LiBC was further treated with a high temperature for 10 h to produce four modified samples: Sample II (pellet, 800°C), Sample III (powder, 800°C), Sample IV (powder, 600°C), and Sample V (powder wrapped in Al foil, 600°C). In order to avoid the contamination by Al foil, the treatment temperature of Sample V was set as 600°C, which was 60°C lower than the melting point of Al. The atomic content of Al was measured by EDS, and only a trace amount (0.01%) of Al was detected in Sample V, as well as Sample I for comparison, indicating that the existence of Al foil did not contaminate the sample.

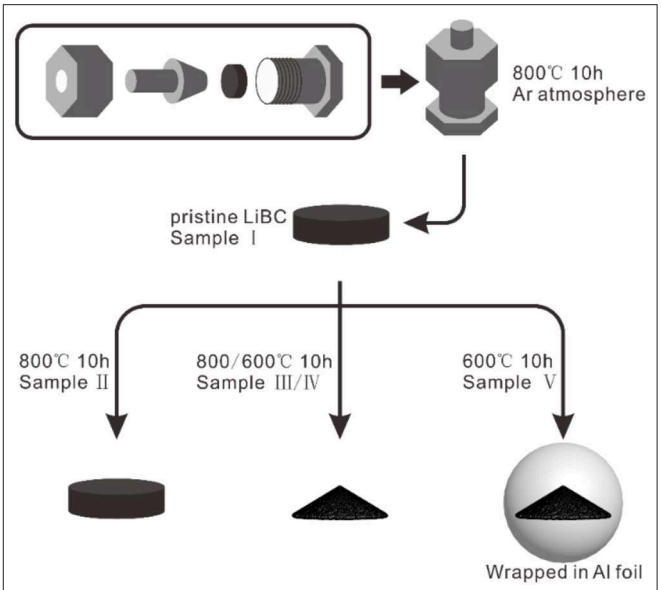

FIGURE 1 | Schematic diagram of LiBC synthesis within a stainless steel vessel and high-temperature treatment for pristine LiBC.

Material Characterization

The crystal structures of LiBC samples were characterized by power X-ray diffraction (XRD, Bruker D2 PHASER) with Cu Kα radiation. The vibration modes were measured using a Raman imaging microscope (Thermo fisher Scientific DXRxi) with a laser wavelength of 532 nm. The morphology was observed through scanning electron microscopy (SEM, Phenom ProX, 10 kV).

Electrochemical Measurements

In a glove box filled with Ar gas (H2O, O2 < 1 ppm), a certain amount of PTFE powder was weighted, and then the LiBC powder was weighted with the mass ratio of LiBC:PTFE = 9:1. Here, the PTFE powder was not convenient to weight for its high viscosity, and we did not add conductive agent in the working electrode in order to eliminate the capacity influence of acetylene black. The mixture was well-mixed with a spoon and ground to achieve a composition film in a mortar. The film was punched into circular pieces with diameters of 4 mm, which were roughly pressed on a stainless-steel mesh. A folded titanium plate was used to nip the electrode, which was firmly pressed with a pressure of 10 T outside the glove box. Finally, the pressed electrode was taken out and preserved in the glove box. The working electrode was assembled in a coin cell (CR2025) with an electrolyte of 1M LiClO4 in ethylene carbonate/diethyl carbonate (EC/DEC 1:1 by volume) and a separator (Celgard 2400, 25 μm) in an Ar atmosphere. At a room temperature of 25°C, galvanostatic measurements were carried out with a battery charge/discharge system from Hokuto Denko Corp., and EIS measurements were performed on an electrochemical workstation (Biologic VSP300).

RESULTS AND DISCUSSION

Figure 2 shows the SEM images of five LiBC samples. There are many large flakes in Sample I-IV, while Sample V appears as a small-particle assembly. According to the XRD patterns in **Figure 3A**, five samples mainly consist of LiBC (JCPDS 85-2010) indexed with a space group symmetry of $P6_3/mmc$, except for a little graphite and Li_2O.

The lattice parameters of five LiBC samples were calculated through the cell refinement with XRD patterns, as listed in

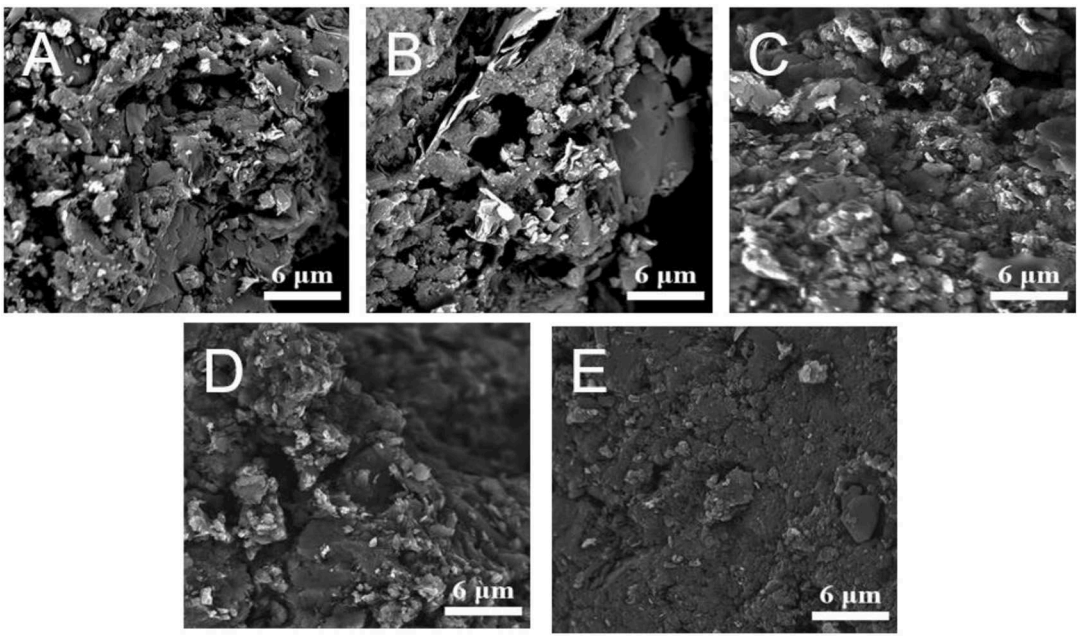

FIGURE 2 | The SEM images of five LiBC samples, **(A)** I. Pristine LiBC, **(B)** II. 800-pellet, **(C)** III. 800-powder, **(D)** IV. 600-powder, and **(E)** V. 600-powder-Al.

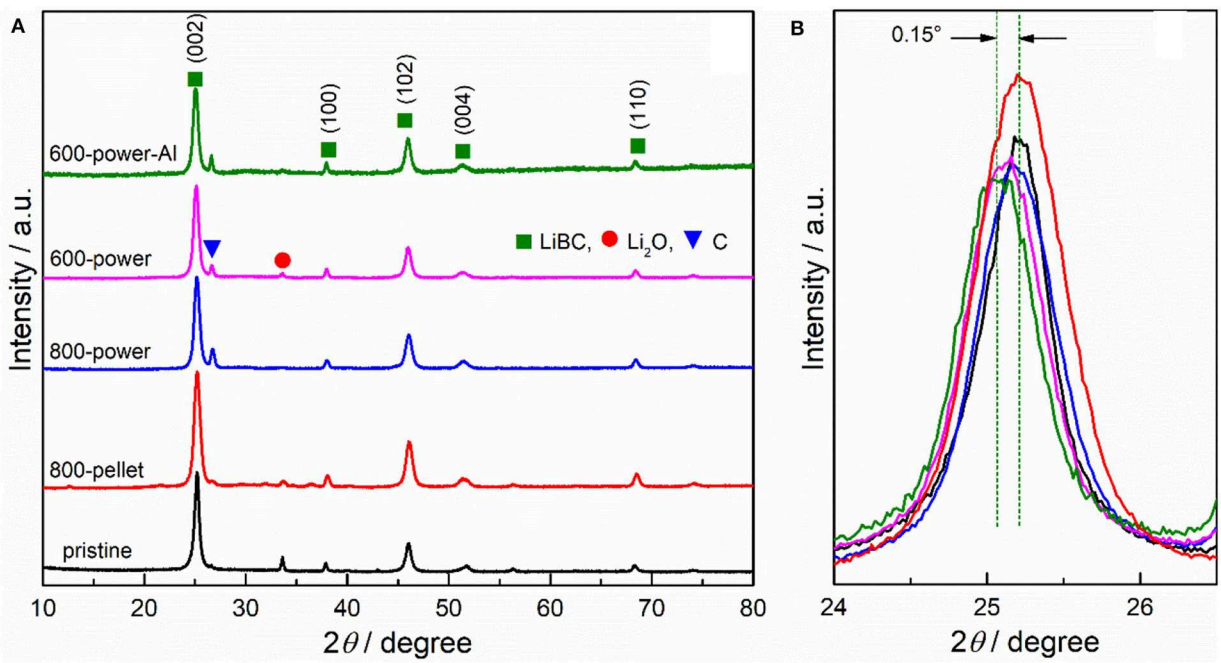

FIGURE 3 | (A) The XRD patterns for five LiBC samples and **(B)** the enlarged views for Peak (002).

Table 1. As the (002) peak shifted to the small angle in **Figure 3B**, the lattice parameter c evidently increased after high-temperature treatment, especially for Sample V, but rarely changed for the lattice parameter a. Thereby, the interlayer distance should be increased, while the intra-layer structure might be retained.

In the Raman spectra of five LiBC samples in **Figure 4A**, there are five pronounced bands at frequencies of 171, 546, 826, 1,167, and 1,254 cm^{-1}, which correspond to E_{2g} (BC planes slide against each other, Li at rest), B_{2u} (Li layers vibrate against each other along c), B_{1g} (symmetric vibration of BC layers along c, Li at rest), E_{2g} (B-C bond stretching mode, even displacement of BC layers), and E_{1u} (B-C bond stretching mode, odd displacement of BC layers), respectively (Hlinka et al., 2003a,b; Renker et al., 2004). The strong asymmetric bands at 1,689 and 2,511 cm^{-1} seem to correspond well to double frequency of the B-C puckering mode and the B-C bond stretching mode, respectively (Fogg et al., 2003). After high-temperature treatment, the 1,254 cm^{-1} peak changed evidently compared with the 1,167 cm^{-1} peak, as well as the other two peaks at 546 and 826 cm^{-1}, which was also observed in the early literature (Hlinka et al., 2003a). As shown in **Figure 4B**, the 1,254 cm^{-1} peak was lower for Sample III in powder vs. Sample II in pellet, for Sample III at 800°C vs. Sample IV at 600°C, and for Sample IV without wrapping vs. Sample V wrapped in Al foil. In our previous work (Jia et al., 2018), we also observed the decrease of the 546, 826, and 1,254 cm^{-1} peaks when the LiBC material was delithiated electrochemically. Thereby, the decreasing peak might be attributed to the lithium loss of LiBC through evaporation at high temperature, especially for powder, higher temperature, and no wrapping.

In our previous work (Jia et al., 2018), the (002) peak shifted to a larger angle with charging (delithiation) and moved back with discharging (lithiation) according to the *in situ* XRD results, indicating that the distance between B–C layers increases with the Li-ion content. In this work, the (002) peak shifted to a smaller angle with lithium evaporation by high temperature treatment, which was opposite to the previous electrochemical result at room temperature. Therefore, the high temperature treatment should cause the crystal structure change of LiBC besides the lithium evaporation.

TABLE 1 | Lattice parameters a and c for five LiBC samples according to the XRD patterns.

Sample	a/Å	c/Å
I. Pristine LiBC	2.744	7.064
II. 800-pellet	2.738	7.068
III. 800-powder	2.741	7.073
IV. 600-powder	2.741	7.091
V. 600-powder-Al	2.742	7.105

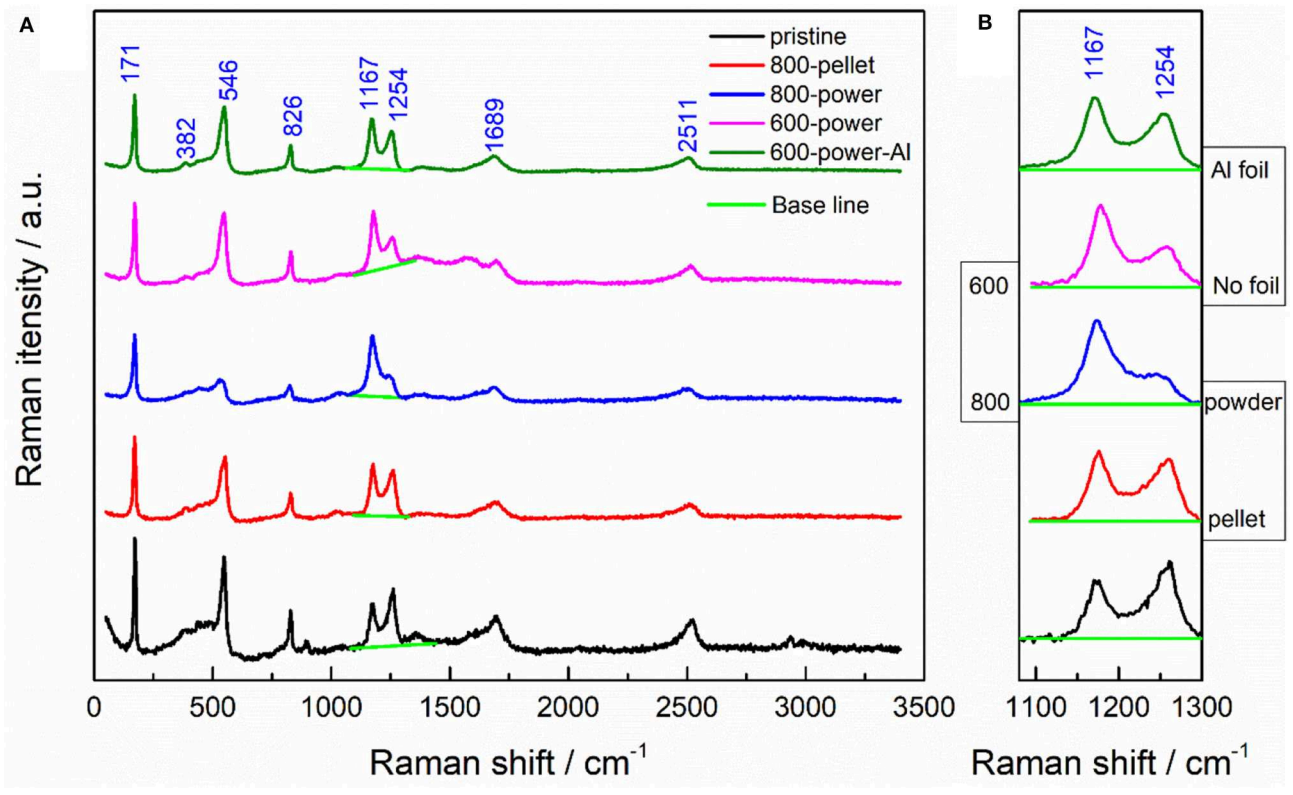

FIGURE 4 | (A) The Raman spectra of five LiBC samples. **(B)** The enlarged views for two Raman peaks after the baseline subtraction.

Galvanostatic measurements were conducted for five LiBC samples, as shown in **Figure 5**. The initial charge capacity was 305, 304, 369, 340, and 419 mAh/g for Sample I-V, respectively, and they delivered a reversible capacity of 218, 230, 291, 259, and 353 mAh/g in the 10th cycle, respectively. Here, the initial capacity is larger than the reversible capacity, which might be due to structural evolution. In the first cycle, the initial structure is a good layered structure, but the BC layer will be distorted through charging, which cannot be completely restored in the following cycles. The large polarization should be owing to the structure evolutions of LiBC during (dis)charging. During cycling, the charge capacity is nearly the same as the discharge capacity of LiBC, and the coulomb efficiency is about 100%. In comparison, Sample III of powder has a larger reversible capacity than that of Sample II of pellet. And the capacity of Sample IV at 600°C is smaller than that of Sample III at 800°C. However, the capacity of sample V wrapped in Al foil is larger than not only Sample IV with the same temperature, but also Sample III

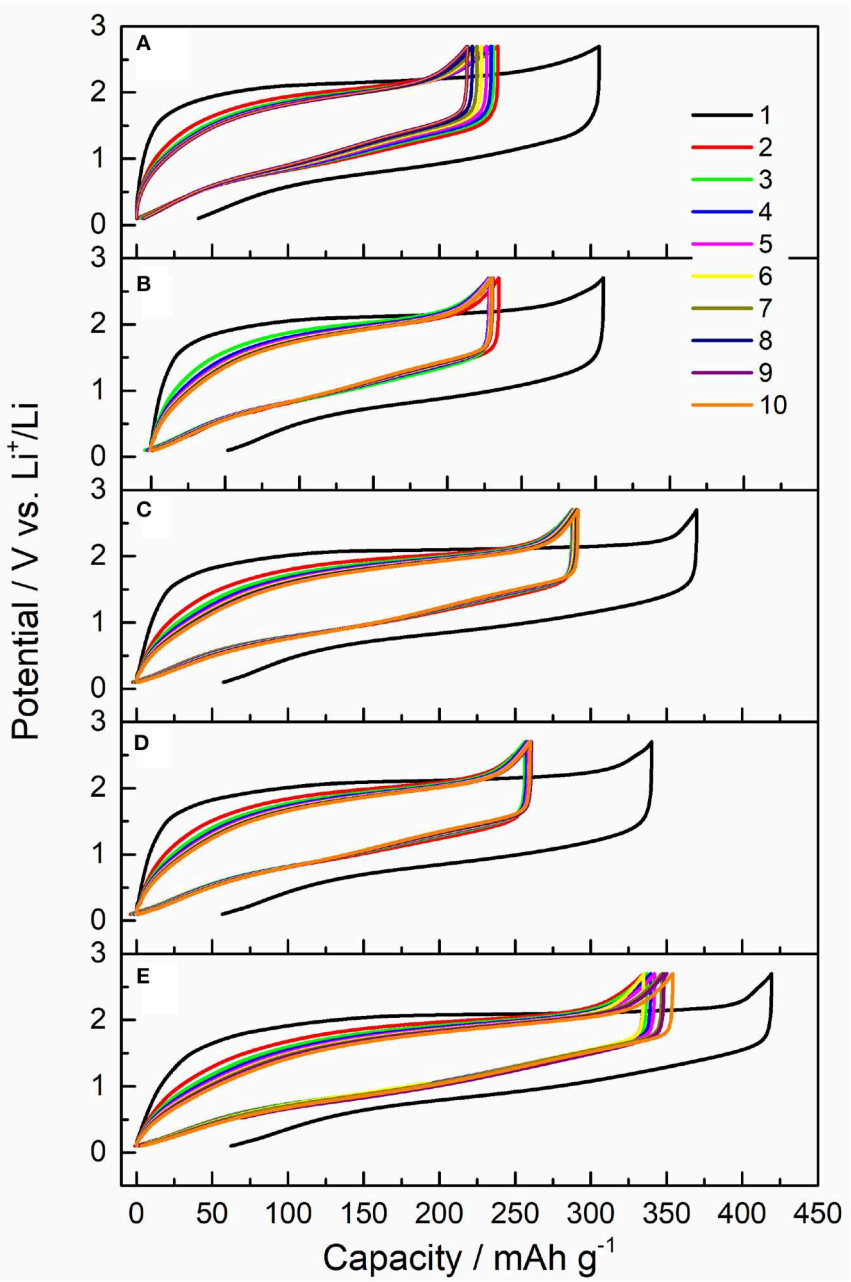

FIGURE 5 | The charge-discharge curves of initial 10 cycles for five samples, **(A)** I. Pristine LiBC, **(B)** II. 800-pellet, **(C)** III. 800-powder, **(D)** IV. 600-powder, and **(E)** V. 600-powder-Al, with a current of 0.05 C and a voltage range of 0.1–2.7 V.

with a higher temperature. For Sample V has the largest interlayer distance, the increased capacity of LiBC should be attributed to the changed crystal structure. Notably, according to the Raman result in **Figure 4**, the high temperature treatment at 800°C made Sample III have a lowest lithium content, which would decrease the interlayer distance, as reported in our previous work (Jia et al., 2018). Thus, the capacity of Sample III is higher than that for Sample IV, although Sample III has a smaller interlayer distance.

The corresponding dQ/dV curves were plotted for the initial 10 cycles, as shown in **Figure 6**. For the initial cycle, there was an oxidation peak at ca. 2.1 V and a reduction peak at ca. 0.8 V, and the oxidation peak was very sharp and high, corresponding to the flat plateau of initial charge. In the second cycle, the oxidation peak decreased dramatically and moved to the low potential. The reduction peak was also evidently reduced and a new reduction peak emerged on its right shoulder. In the next cycles, the oxidation peak became short and broad gradually, and it shifted to ca. 1.95 V in the tenth cycle. The reduction peak at ca. 0.8 V decreased gradually, and the new reduction peak grew up evidently. Compared with the other four samples, the reduction peak at ca. 0.8 V decreased quite a little for Sample V, the new reduction peak of Sample V had a highest potential of ca. 1.61 V and a smallest height relative to the reduction peak at ca. 0.8 V. Clearly, the capacity of Sample V was mainly attributed to the couple of redox peaks at ca. 1.95 and ca. 0.8 V, while the new reduction peak made a considerable contribution to the capacity of the other four samples, so the larger capacity of Sample V might be related to the stable structure during the cycles. By the way, the strong interaction between the Li 2s electron and the B 2pz orbital should give rise to the high redox potential compared with acetylene black, that is, the B atoms should be reduced during discharging and oxidized back during charging.

To investigate the electrochemical kinetics of LiBC, we characterized Sample I and Sample V by electrochemical impedance spectroscopy (EIS). After 10 cycles, the LiBC electrodes took a rest for 5 h as State 1#, with a discharge to 0.1 V as State 2#, a charge to 2.7 V as State 3#, and a discharge to 0.1 V as State 4#, in which the current was 22.5 mA/g for both charge and discharge, as shown in **Figure 7A**. The Nyquist plots of Sample I and Sample V were plotted in the top and bottom of **Figure 7B**, respectively, and their enlarged views were presented in **Figures 7C,D**, respectively. All EIS spectra appear as one semicircle in the high frequency followed by a tilted line in the low frequency, which was evidently curved near the semicircle for Sample V. Compared with the discharge state, the semicircle was nearly double and the tilted line was quite long

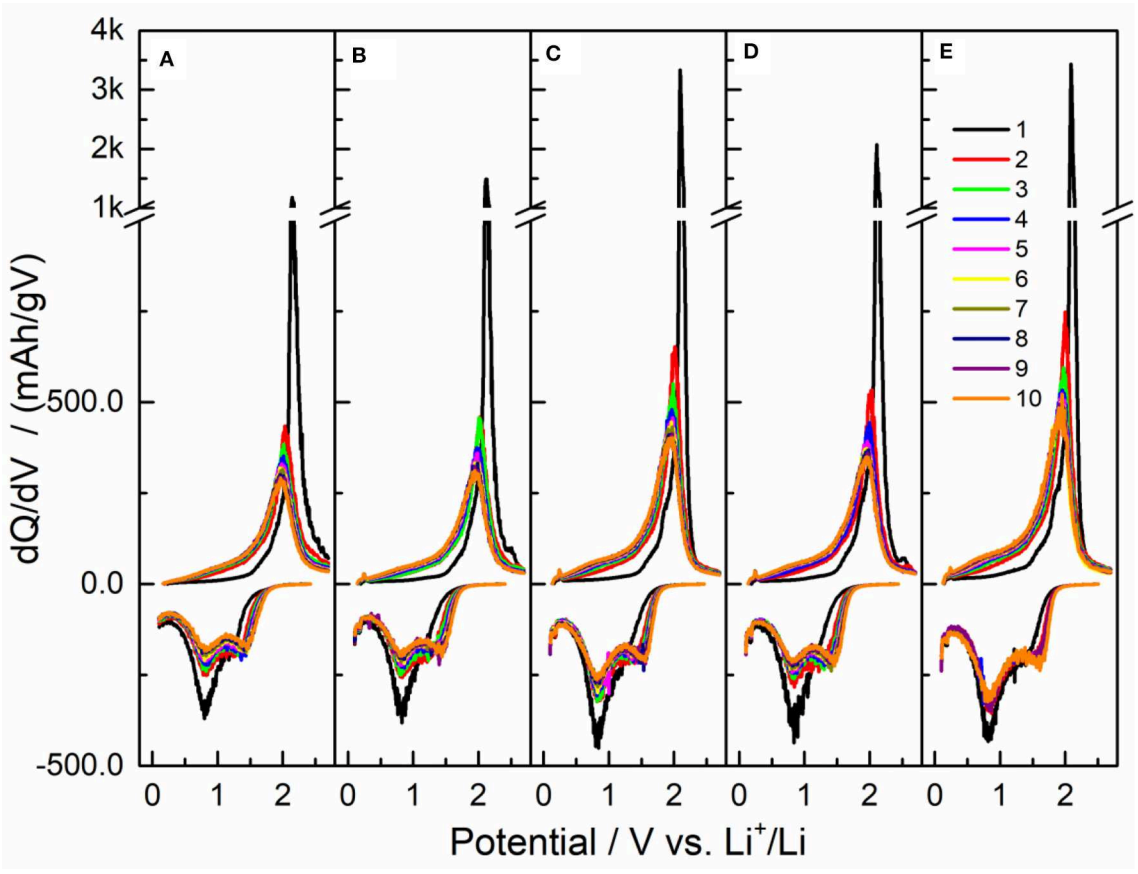

FIGURE 6 | The dQ/dV curves of the initial 10 charge-discharge cycles in **Figure 5** for five samples, **(A)** I. Pristine LiBC, **(B)** II. 800-pellet, **(C)** III. 800-powder, **(D)** IV. 600-powder, and **(E)** V. 600-powder-Al.

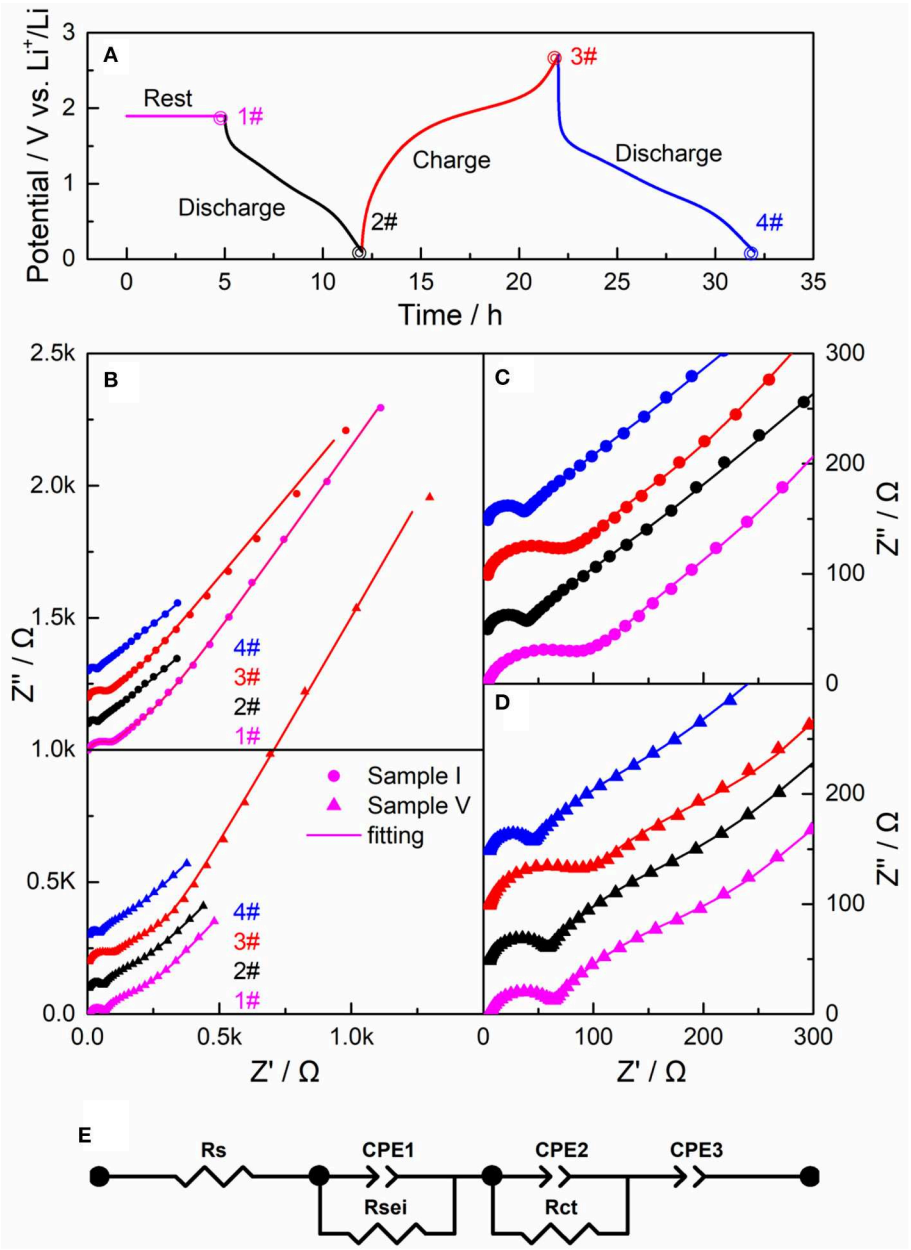

FIGURE 7 | (A) The electrochemical measurements after 10 cycles as rest for 5 h (1#), discharge to 0.1 V (2#), charge to 2.7 V (3#), and discharge to 0.1 V (4#) with a current of 0.05 C. **(B)** The impedance spectra of Sample I. Pristine LiBC and Sample V. 600-powder-Al at State 1# (magenta), State 2# (black), State 3# (red), and State 4# (blue), and the corresponding enlarged views in **(C,D)**. **(E)** The equivalent circuit to fit the impedance spectra in **(B–D)** as the curve lines.

for the charged state. To further analyze the EIS spectra, we fitted them with an equivalent circuit model, as shown in **Figure 7E**, in which Rsei and Rct could be assigned to the resistance of the SEI layer and the charge transfer resistance, respectively (Nam et al., 2013). As fitting the result in **Table 2**, the Rsei values are comparable between two samples, and the Rct value of Sample V is over three times of that for Sample I. expect for State 1#. Thereby, the electrical conductivity of LiBC was reduced considerably through the high-temperature treatment, indicating the modification of crystal structure.

Furthermore, we proposed a potential mechanism for high-temperature treatment of LiBC under different conditions. As shown in **Figures 8A,B**, the lithium ions in the powder could be easily evaporated though the particle surface at a high temperature of 800°C, while the large pellet would confine the lithium ions inside, so the lithium content of Sample III should be reduced more than that of Sample II. For the lithium evaporation that would be enhanced at a higher temperature, Sample III at 800°C would lose more lithium ions than Sample IV. As shown in **Figure 8C**, the wrapped Al foil would significantly block the

TABLE 2 | The fitting results within an equivalent circuit for the impedance spectra in **Figure 7**.

State / parameter	1#	2#	3#	4#
Rsei -I (Ω)	91.88	29.75	75.27	27.44
Rsei -V (Ω)	53.51	48.51	76.12	35.02
Rct -I (Ω)	97.29	25.08	42.48	18.65
Rct -V (Ω)	111.9	90.13	172.2	59.53

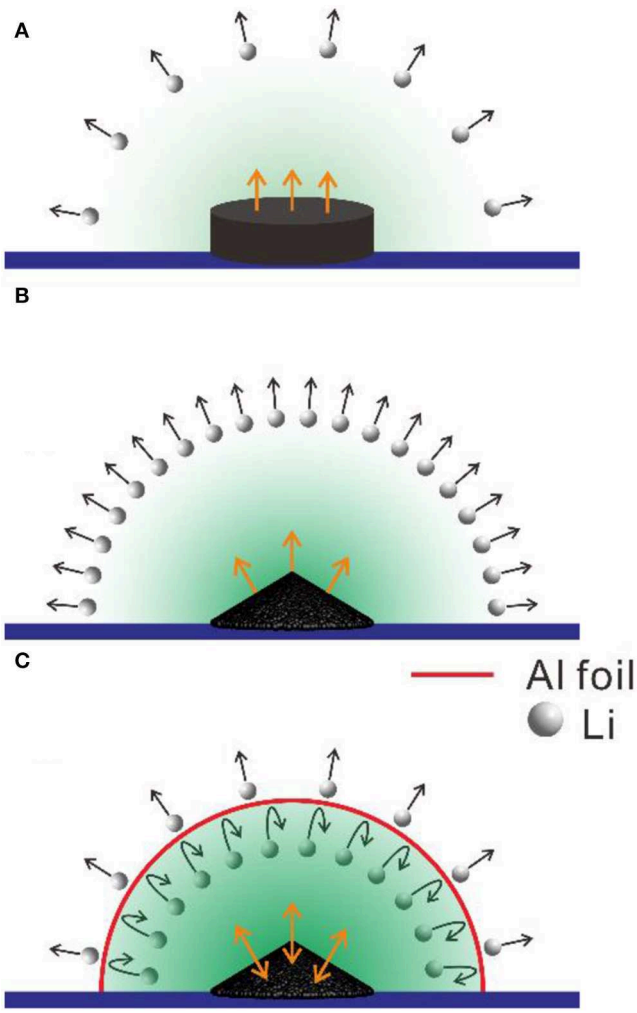

FIGURE 8 | Schematic diagram of lithium evaporation from LiBC during high-temperature treatment under different conditions. **(A)** pellet, **(B)** power, and **(C)** power wrapped in Al foil.

lithium evaporation in forming a lithium atmosphere, and the lithium ions would be exchanged between the LiBC and the atmosphere, which would result in the evolution of the LiBC structure, as shown in **Table 1**. This mechanism could be verified by the lithium content analyzed from the Raman spectra in **Figure 4B**. In the early literature, the interlayer distance of LiBC was slightly decreased when increasing the lithium content from raw materials or synthesizing under a high hydrogen pressure. (Kudo et al., 2005; Fogg et al., 2006) Similarly, it was modified through the lithium evaporation and exchange in the high-temperature treatment here, which improved the capacity of LiBC in Li-ion batteries.

CONCLUSIONS

In this work, a pristine LiBC material was treated with a high temperature to obtain four modified LiBC samples. According to the XRD/Raman/EIS results, the treatment would increase the interlayer distance, while reducing lithium content and electrical conductivity. In Li-ion batteries, a reversible capacity of 353 mAh/g was delivered by a modified LiBC sample that was treated at 600°C for 10 h in a powder form wrapped with an Al foil, compared with 218 mAh/g for the pristine LiBC. The better electrochemical performance might be attributed to the changed crystal structure, which appeared more stable during the electrochemical reaction. Thereby, we proposed that the interlayer distance of LiBC was modified through the lithium evaporation and exchange in the high-temperature treatment, which improved the capacity of LiBC in Li-ion batteries. This method would make the LiBC material a more promising anode material in Li-ion batteries.

DATA AVAILABILITY STATEMENT

All datasets generated for this study are included in the article/supplementary material.

AUTHOR CONTRIBUTIONS

YC directed the project and DL took charge of this investigation. QY optimized in synthesis, analyzed the data, and authored the manuscript. All authors contributed to the discussion.

FUNDING

This work was financially supported by Natural Science Foundation of Hainan Province (Nos. ZDYF2019012, 2018CXTD332, and HD-SYSZX-201802), National Natural Science Foundation of China (Nos. 21603048 and 51362009), the Science and technology development special fund project (No. ZY2018HN09-3), and the Hainan University's Scientific Research Foundation (No. kyqd1545).

REFERENCES

An, J. M., and Pickett, W. E. (2001). Superconductivity of MgB_2: covalent bonds driven metallic. *Phys. Rev. Lett.* 86, 4366–4369. doi: 10.1103/PhysRevLett.86.4366

Armand, M., and Tarascon, J. M. (2008). Building better batteries. *Nature* 451, 652–657. doi: 10.1038/451652a

Belasfar, K., Houmad, M., Boujnah, M., Benyoussef, A., and Kenz, A. E. L. (2020). First-principles study of BC_3 monolayer as anodes for lithium-ion and sodium-ion batteries applications.

J. Phys. Chem. Solids 139:109319. doi: 10.1016/j.jpcs.2019.109319

Bharathi, A., Balaselvi, S. J., Premila, M., Sairam, T. N., Reddy, G. L. N., Sundar, C. S., et al. (2002). Synthesis and search for superconductivity in LiBC. *Solid State Commun.* 124, 423–428. doi: 10.1016/S0038-1098(02)00474-X

Chevallier, F., Poli, F., Montigny, B., and Letellier, M. (2013). *In situ* Li nuclear magnetic resonance observation of the electrochemical intercalation of lithium in graphite: second cycle analysis. *Carbon* 61, 140–153. doi: 10.1016/j.carbon.2013.04.078

Fogg, A. M., Chalker, P. R., Claridge, J. B., Darling, G. R., and Rosseinsky, M. J. (2003). LiBC electronic, vibrational, structural, and low-temperature chemical behavior of a layered material isoelectronic with MgB_2. *Phys. Rev. B* 67, 841–845. doi: 10.1103/PhysRevB.67.245106

Fogg, A. M., Darling, G. R., Claridge, J. B., Meldrum, J., and Rosseinsky, M. J. (2008). The chemical response of main-group extended solids to formal mixed valency: the case of Li_xBC. *Phil. Trans. R. Soc. A* 366, 55–62. doi: 10.1098/rsta.2007.2139

Fogg, A. M., Meldrum, J., Darling, G. R., Claridge, J. B., and Rosseinsky, M. J. (2006). Chemical control of electronic structure and superconductivity in layered borides and borocarbides: understanding the absence of superconductivity in Li_xBC. *J. Am. Chem. Soc.* 128, 10043–10053. doi: 10.1002/chin.200645013

Hlinka, J., Gregora, I., Pokorný, J., Pronin, A. V., and Loidl, A. (2003a). Polarized raman spectroscopy of LiBC: possible evidence for lower crystal symmetry. *Phys. Rev. B* 67:020504. doi: 10.1103/PhysRevB.67.020504

Hlinka, J., Železný, V., Gregora, I., Pokorný, J., Fogg, A. M., Claridge, J. B., et al. (2003b). Vibrational properties of hexagonal LiBC: infrared and raman spectroscopy. *Phys. Rev. B* 68:220510. doi: 10.1103/PhysRevB.68.220510

Jia, J., Chen, S., Yang, Q., Feng, X., and De Li (2018). Crystallinity-dependent capacity of a LiBC anode material in Li-ion batteries. *Phys. Chem. Chem. Phys.* 20, 28176–28184. doi: 10.1039/c8cp05561k

Joshi, R. P., Ozdemir, B., Barone, V., and Peralta, J. E. (2015). Hexagonal BC_3: a bobust electrode material for Li, Na, and K ion batteries. *J. Phys. Chem. Lett.* 6, 2728–2732. doi: 10.1021/acs.jpclett.5b01110

Kalkan, B., and Ozdas, E. (2019). Staging phenomena in lithium-intercalated boron-carbon. *ACS Appl. Mater. Interfaces* 11, 4111–4122. doi: 10.1021/acsami.8b19142

King, T. C., Matthews, P. D., Glass, H., Cormack, J. A., Holgado, J. P., Leskes, M., et al. (2015). Theory and practice: bulk synthesis of C_3B and its H_2- and Li-storage capacity. *Angew. Chem.* 127, 6017–6021. doi: 10.1002/ange.201412200

King, T. C., Matthews, P. D., Holgado, J. P., Jefferson, D. A., Lambert, R. M., Alavi, A., et al. (2013). A single-source route to bulk samples of C_3N and the co-evolution of graphitic carbon microspheres. *Carbon* 64, 6–10. doi: 10.1016/j.carbon.2013.04.043

Krumeich, F., Worle, M., Reibisch, P., and Nesper, R. (2014). Characterization of LiBC by phase-contrast scanning transmission electron microscopy. *Micron* 63, 64–68. doi: 10.1016/j.micron.2013.10.012

Kudo, T., Nakamori, Y., Orimo, S-I., Badica, P., and Togano, K. (2005). Hydrogen effects on synthesis processes and electrical resistivities of LiBC. *J. Japan Inst. Metals* 69, 433–428. doi: 10.2320/jinstmet.69.433

Kuzubov, A. A., Fedorov, A. S., Eliseeva, N. S., Tomilin, F. N., Avramov, P. V., and Fedorov, D. G. (2012). High-capacity electrode material BC_3 for lithium batteries proposed byab initiosimulations. *Phys. Rev. B* 85:195415. doi: 10.1103/PhysRevB.85.195415

Langer, T., Dupke, S., Dippel, C., Winter, M., Eckert, H., and Pöttgen, R. (2012). LiBC – synthesis, electrochemical and solid-state NMR investigations. *Z. Naturforsch. B* 67, 1212–1220. doi: 10.5560/znb.2012-0223

Li, D., Dai, P., Chen, Y., Peng, R., Sun, Y., and Zhou, H. (2018). Lithium borocarbide LiBC as an anode material for rechargeable Li-ion batteries. *J. Phys. Chem. C* 122, 18231–18236. doi: 10.1021/acs.jpcc.8b03763

Nam, K. M., Shin, D. H., Jung, N., Joo, M. G., Jeon, S., Park, S. M., et al. (2013). Development of galvanostatic fourier transform electrochemical impedance spectroscopy. *Anal. Chem.* 85, 2246–2252. doi: 10.1021/ac303108n

Ohzuku, T., Iwakoshi, Y., and Sawai, K. (1993). Formation of lithium-graphite intercalation compounds in nonaqueous electrolytes and their application as a negative electrode for a lithium ion (shuttlecock) cell. *Cheminform* 140, 2490–2497. doi: 10.1149/1.2220849

Renker, B., Schober, H., Adelmann, P., Schweiss, P., Bohnen, K. P., and Heid, R. (2004). Lattice dynamics of LiBC. *Phys. Rev. B* 69:052506. doi: 10.1103/PhysRevB.69.052506

Shan, H., Li, X., Cui, Y., Xiong, D., Yan, B., Li, D., et al. (2016). Sulfur/nitrogen dual-doped porous graphene aerogels enhancing anode performance of lithium ion batteries. *Electrochi Acta* 205, 188–197. doi: 10.1016/j.electacta.2016.04.105

Souptel, D., Hossain, Z., Behr, G., Löser, W., and Geibel, C. (2003). Synthesis and physical properties of LiBC intermetallics. *Solid State Commun.*125, 17–21. doi: 10.1016/S0038-1098(02)00702-0

Van Noorden, R. (2014). The rechargeable revolution: a better battery. *Nature* 507, 26–28. doi: 10.1038/507026a

Way, B. (2010). The effect of boron substitution in carbon on the intercalation of lithium in $Li_x(B_zC_{1-z})_6$. *J. Electrochem. Soc.* 141, 907–912. doi: 10.1002/chin.199431008

Woerle, M., Nesper, R., Mair, G., Schwarz, M., and Schnering, H. G. V. (1995). ChemInform abstract: LiBC. A completely intercalated heterographite. *Z. Anorg. Allg. Chem.* 621, 1153–1159. doi: 10.1002/chin.199543010

Xiong, D., Li, X., Bai, Z., and Lu, S. (2018). Recent advances in layered $Ti_3C_2T_x$ MXene for electrochemical energy storage. *Small* 14:e1703419. doi: 10.1002/smll.201703419

Xu, Q., Ban, C., Dillon, A. C., Wei, S. H., and Zhao, Y. (2011). First-principles study of lithium borocarbide as a cathode material for rechargeable Li ion batteries. *J. Phys. Chem. Lett.* 2, 1129–1132. doi: 10.1021/jz200440m

Zhao, L., Klavins, P., and Liu, K. (2003). Synthesis and properties of hole-doped $Li_{1-x}BC$. *J. Appl. Phys.* 93, 8653–8655. doi: 10.1063/1.1556285

Conflict of Interest: The authors declare that the research was conducted in the absence of any commercial or financial relationships that could be construed as a potential conflict of interest.